Multimodal visualization of adult stem cells in inner ear and brain pathology

Schomann, T.

Cover Page

Universiteit Leiden

Author: Schomann, T.
Title: Multimodal visualization of adult stem cells in inner ear and brain pathology
Issue Date: 2019-05-16

Chapter 1

General introduction

Hearing, development, anatomy and physiology

Hearing is one of the five senses of perception in humans and most other vertebrates. In the process of hearing, sound pressure waves are converted into electrical signals, that are propagated by neurons to the brain where these signals are subsequently processed.

During embryonic development the structures of the inner ear arise from the otic placode, an ectodermal thickening in the head region of the embryo.

The otic placode, like other neurogenic placodes, develops at the border of the neural plate [1]. All epibranchial neurogenic placodes originate in a common pre-placodal region slightly more lateral than the neural crest (NC) and form discrete areas of columnar epithelium derived from non-neural ectoderm [2]. During development, these placodes give rise to neuroepithelium in the sensory organs of the vertebrate.

The olfactory epithelium in the nose is generated by the olfactory placode and the lens of the eye is produced by cells of the lens placode (or optic placode). Similarly, the audiovestibular system originates from the otic placode. Together with the NC, the otic placode also contributes to the peripheral nervous system of the respective sensory organ. The otic placode invaginates and undergoes a complex morphogenesis into the inner ear [3, 1].

The fully mature hearing organ consists of three major parts: the outer ear, the middle ear, and the inner ear (Fig. 1). The outer ear consists of the pinna (or auricle; Fig. 1A) and the external auditory meatus (or outer ear canal; Fig. 1B), which focus sound, an audible mechanical wave of pressure and displacement, and conduct it to the tympanic membrane (or eardrum; Fig. 1C). In the middle ear, sound waves are propagated and transformed through vibrations of the comparatively large, low-impedance tympanic membrane to the smaller, high-impedance oval window of the cochlea (impedance increase: 18.75 times in humans) by means of the three auditory ossicles (Fig. 1D): the malleus (hammer; impedance increase: 2.1 times in humans), incus (anvil), and stapes (stirrup) [4]. The auditory ossicles function as an acoustic impedance transformer that converts sound energy from low-impedance air to the high-impedance cochlear fluids (Fig. 1E) [5]. This is achieved by a piston-like movement of the stapes' footplate in the oval window, which generates pressure

waves that travel through the fluid-filled compartments of the cochlea. In humans, the total transformer ratio of the middle ear amounts to 82.5 times, which also includes the 2.1-times velocity decrease (2.1^2 = 4.4 times) [4].
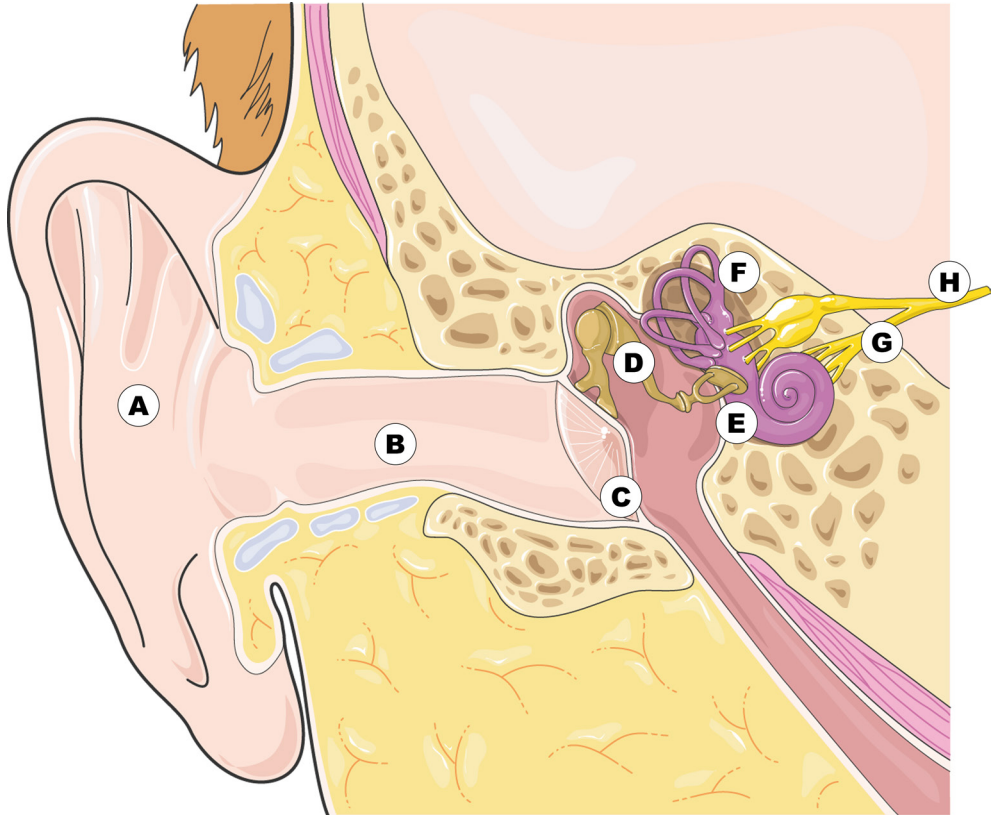
Fig. 1: The ear. **A:** pinna (auricle), **B:** external auditory meatus (ear canal), **C:** tympanic membrane (eardrum), **D:** auditory ossicles: the malleus (hammer), incus (anvil), and stapes (stirrup), **E:** cochlea, **F:** vestibular system, **G:** auditory nerve, **H:** vestibulocochlear nerve. Picture adapted from "Ear" [6].

The cochlea is a snail-shaped, bony structure that houses the neurosensory organ of hearing (organ of Corti) and forms one of the two major structures of the inner ear. The other major apparatus of the inner ear is the vestibular system, containing the organs of balance (Fig. 1F).

In humans, the cochlea coils approximately 2.5 turns around its central axis, while in other mammals the number of turns slightly varies. The cochlea in mice has 2 turns and in guinea pigs it has approximately 4 turns (Fig. 2A). In humans and other mammals, the cochlea consists of three fluid-filled compartments: the scala vestibuli,

scala tympani and scala media (Fig. 2B). The scala vestibuli spirals upwards to the helicotrema at the apex of the cochlea, where it is connected to the scala tympani which conversely spirals downwards. Both compartments are broad near the base and become more narrow towards the apex. They are filled with perilymph, which is characterized by a high sodium concentration (~140 mM) and low levels of potassium (4-5 mM) and resembles the electrolyte composition of the cerebrospinal fluid. In between these two perilymph-filled scalae, the scala media (or cochlear duct) is located. It is filled with endolymph, which has low levels of sodium (~1 mM) and a high potassium concentration (~150 mM). The scala media contains the organ of Corti, which houses the sensory receptors of hearing, the cochlear hair cells, i.e., one row of inner hair cells (IHCs) and three to four rows of outer hair cells (OHCs), and other highly specialized cells, such as Deiters' cells, Hensen's cells and Claudius' cells (Fig. 2C).

In the scala vestibuli, the traveling pressure wave, which is generated by the movement of the stapes, causes a vibration of the perilymphatic fluid towards the round window [4]. This initiates a displacement on the basilar membrane from base to apex, whereby pattern and positioning of the wave depends upon the frequency of the stimulus. In response to the vibrations of the basilar membrane, the entire organ of Corti is moved up and down [7]. Depending on the frequency, the location of maximal displacement of the basilar membrane is different and relies on its physical mechanics and the composition of the cochlear fluids [5]. At the base of the cochlea, high-frequency stimuli lead to a maximal displacement of the basilar membrane, since it possesses a lower mass and higher stiffness than in the more apical regions [7, 5]. Consequently, low-frequency stimuli lead to maximal displacement towards the apex of the cochlea.

The displacement of the basilar membrane pushes the stereocilia of the OHCs against the tectorial membrane [4]. Due to this tension on the tips of the stereocilia, the stereocilia deflect, whereupon the mechanoelectrical transduction channels open leading to depolarization of the hair cells through influx of potassium from the endolymph [8]. This depolarization results in a release of the neurotransmitter glutamate at the base of the hair cells that evokes an action potential in the synapses of the innervating afferent spiral ganglion neurons (SGNs). After binding of the neurotransmitters to the respective membrane receptors in the synapse, the individual neurons depolarize and an electrical signal is generated.
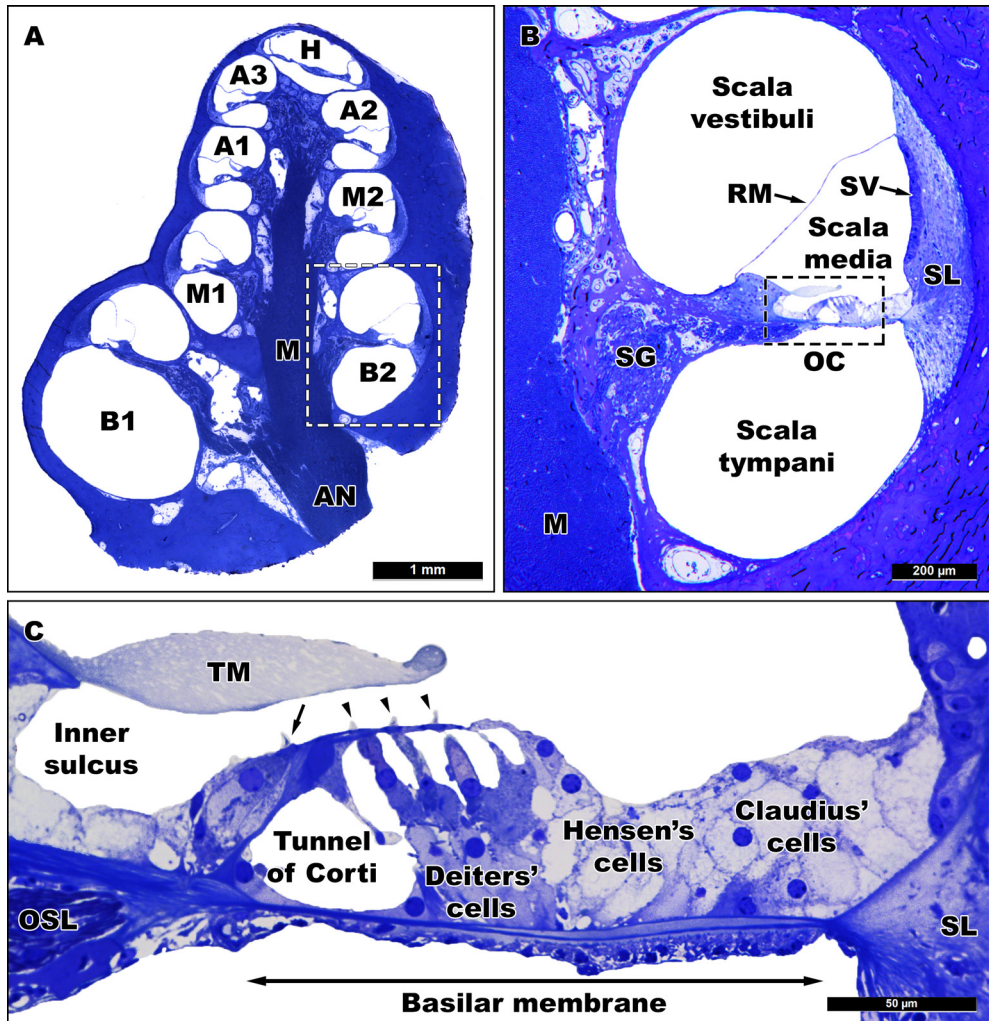
Fig. 2: The guinea pig cochlea and organ of Corti. **A:** Midmodiolar section of a guinea pig cochlea showing all eight scalae. M = modiolus; AN = auditory nerve; B1 = lower basal turn; B2 = upper basal turn; M1 = lower middle turn; and M2 = upper middle turn; A1, A2 and A3 = three apical turns; H = helicotrema. **B:** The upper basal turn (B2) and its scalae. RM = Reissner's membrane; OC = organ of Corti; SG = spiral ganglion; M = modiolus; SL = spiral ligament; SV = stria vascularis. **C:** The organ of Corti contains different highly specialized cells, such as the cochlear hair cells, Deiters' cells, Hensen's cells, Claudius' cells, and the inner sulcus. The organ of Corti is located on the basilar membrane and contains inner hair cells (arrow) and outer hair cells (arrowheads). OSL = osseous spiral lamina; SL = spiral ligament; TM = tectorial membrane.

Small voltage changes are propagated by the SGNs, which form the cochlear nerve within the modiolus. Outside the cochlea, the cochlear nerve joins the vestibular nerve to form the vestibulocochlear nerve, which ends in the brain stem (Fig. 1H). Next, the nerve fibers enter the cochlear nucleus. The signal is then transferred to the trapezoid body, the superior olivary complex, the lateral lemniscus, the inferior colliculus and medial geniculate nucleus before reaching the primary auditory cortex in the brain (Fig. 3).

The propagation of the electrical signal through the neural tracts of the auditory pathway can be measured from relatively large distances using superficial electrodes in humans or subdermal needle electrodes in animals. The time window to record this electrical activity is within milliseconds after the auditory stimulus. Acoustically-evoked auditory brainstem responses (aABRs) can be used to measure and record the propagation of the electrical signal, which gives an indication about the hearing capability of living mammals [9]. The measurements do not require active participation of the subject and are thus a reliable proxy for auditory function in human infants and animals during sleep or anesthesia [10, 11].

After electrical activity is evoked by a broadband acoustic click stimulus, its propagation can be recorded by means of aABR and subsequently visualized as a series of waves using non-invasive or minimally invasive electrodes within 10 milliseconds [12-14]. The first five dominant peaks (I-V) of these waves are evaluated in cats and guinea pigs (Fig. 3A). In these animals, wave I (P1-N1) consists of the first positive peak (P1) and the first negative peak (N1) and represents the combined distal and proximal part of the auditory nerve (Fig. 3B) [15-20]. Waves II-V are generated in the different nuclei in the auditory brainstem [21-23]. The ipsilateral cochlear nucleus generates wave II (P2-N2), while wave III (P3-N3) reflects the activity of the contralateral superior olivary complex and medial nucleus of the trapezoid body. Wave IV represents the combined activity of superior olivary complex and lateral lemniscus (P4-N4) and wave V arises from lateral lemniscus and inferior colliculus (P5).

Recordings of aABRs can help to estimate sensorineural hearing loss (SNHL) by finding the lowest intensity level, at which wave V is present and replicable. SNHL can result from a variety of factors, such as genetic disorder, prolonged exposure to loud noise, ototoxic drug treatment, or simply as a result of ageing, causing degeneration
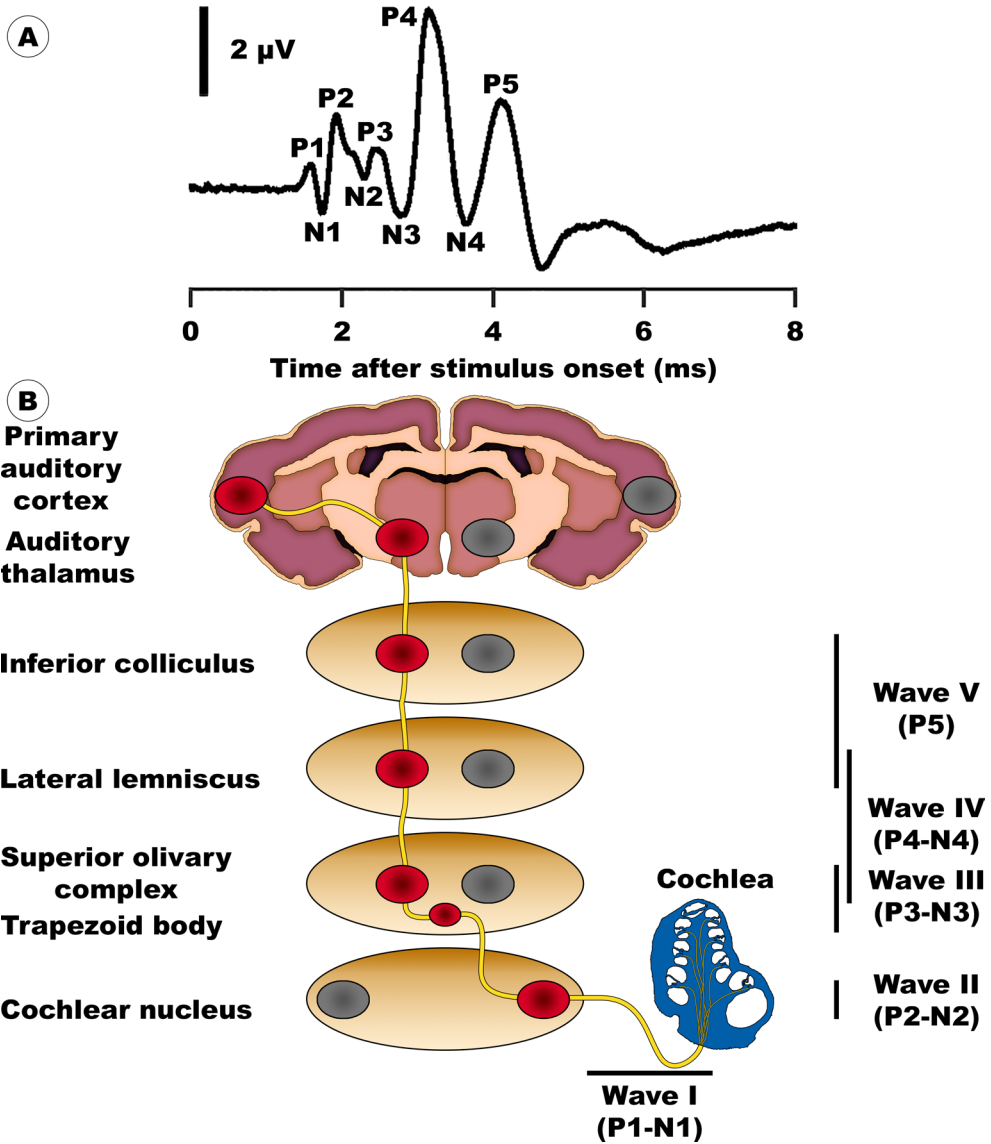
Fig. 3: Schematic drawing of the origin of ABR waves in the guinea pig. **A:** Representation of example of ABR waves with peaks (P) and troughs (N) as measured in a guinea pig. **B:** Waves I – V are generated by the activity of the auditory nerve (yellow), while passing through different areas of the auditory system to deliver the signal to the auditory cortex.

of hair cells and auditory neurons [24]. The degree of neuronal degeneration is of particular significance for hearing-impaired patients. Early on, in ageing or noise-exposed ears, the synapses between the cochlear hair cells and the SGNs degenerate at first and so-called hidden hearing loss develops, which does not affect hearing thresholds but could impair speech understanding in noisy environment [25, 26]. However, once SNHL is diagnosed, affected patients face a rather limited range of therapeutic options, amongst them conventional hearing aids in mild cases or bone-anchored hearing devices and cochlear implants (CIs) in severe cases.

Regarding SNHL, CIs help many hearing-impaired people by partially restoring their sensation of hearing by means of bypassing part of the peripheral auditory system, i.e. the hair cells. The surgically inserted electrode of the CI generates action potentials within the remaining nerve fibers of the spiral ganglion by direct electrical stimulation of the SGNs. Despite considerable progress in CI technology in the past 20 years, there is variability in the performance between individual CI users. Previous studies have suggested that this might be caused by an auditory neuropathy spectrum disorder, which creates site-specific variations of stimulus-dependent activation of neurons [27-29].

Another reason could be an increased distance between the electrodes of the CI and the peripheral projections (dendrites) of the SGNs, which would impair stimulation of the neurons [27, 30-32]. Hence, limiting these variations and increasing the efficiency of the CI is an important aim of current research. Several different approaches have been recently investigated, such as a combination of CI implantation with (neuro) trophic growth factors or stem cell (SC) therapy to improve the hearing of SNHL patients.

Stem cell therapy

Cell-based therapy may counteract the effect of cochlear nerve degeneration [33], although it has to be taken into consideration that, in patients with disabling hearing loss, stem cells will lack (neuro)trophic support of hair cells and perhaps also of non-sensory cells (Fig. 4A-C). Different types of SCs could be applied to support and regenerate the auditory nerve and thereby reducing the distance between CI and

nerve fibers (Fig. 4D). A healthy population of SCs could support the auditory nerve by differentiating into neurons and/or glial cells, which then interact with and help repair the degenerating auditory nerve (Fig. 4E). Another mechanism could be through paracrine effects by stimulation of angiogenesis or support of the microenvironment by reduction of inflammation as shown in other models [34, 35].
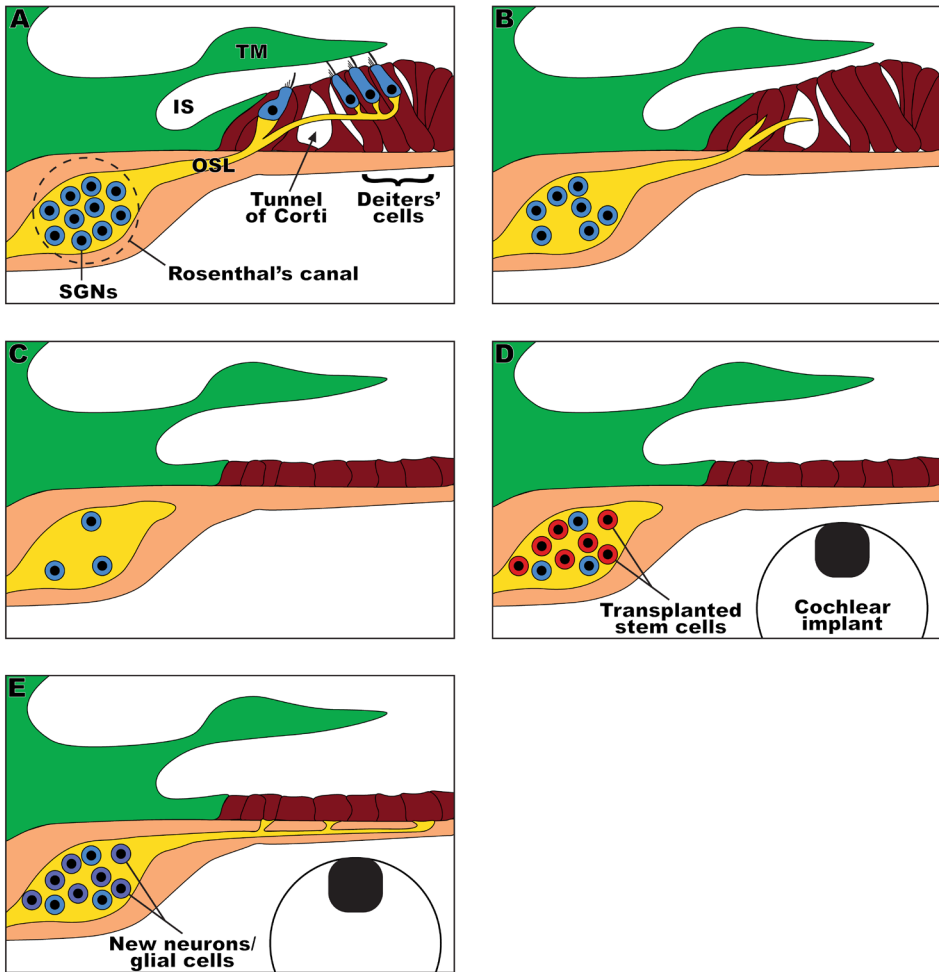

Fig. 4: Schematic drawing of organ of Corti pathology and possible stem cell-based regenerative therapy. **A:** Normal situation with intact inner and outer hair cells (blue), which are innervated by the peripheral projections (dendrites) of the efferent spiral ganglion neurons (SGNs; yellow). TM = tectorial membrane; IS = inner sulcus; OSL = osseous spiral lamina. **B:** Early pathology after damage. Inner and outer hair cells are lost and the amount of SGNs is decreased. **C:** Advanced pathology of the organ of Corti after damage. Organ of Corti is degenerated and replaced by flat epithelium. **D:** Implantation of cochlear implant and transplantation of stem cells (red). **E:** Stem cells support the degenerated nerve fibers and possibly differentiate into new neurons and/or glial cells (purple). This could lead to outgrowth of new nerve fibers and reduce the neural gap with the CI.

For future clinical applications, it would be ideal to have suitable autologous SCs to avoid transplant rejection. Cell-based therapy using stem cells from the neural crest (NC) may represent an attractive therapeutic option [2]. As explained earlier, the NC develops in close proximity to the cranial sensory placodes and interacts with, among others, the otic placode during embryogenesis [36-41, 1]. In addition, gene expression patterns in NC and the otic placode are similar to each other during development [2]. At an early stage of neurulation, the neural plate border is a stripe adjacent to the neural plate and the ectoderm, which co-expresses pre-neural and non-neural ectodermal markers [42-44]. Within the neural plate border region, precursors for neural, NC, epidermal and placodal cells remain interspersed [45, 37]. Similar to the placodal cells, NC cells arise between the newly formed ectoderm and the neural tube in vertebrates after neurulation. This was first described by Wilhelm His in the developing chick embryo as the intermediate cord ('Zwischenstrang') in 1868 [46]. From this tissue, embryonic NC cells migrate out and give rise to several ectodermal and mesodermal cell types in the vertebrate organism [47, 48]. When the first three streams migrate out from the NC, epibranchial progenitor cells converge to form distinct placodes. This suggests a role of NC migration in the individualization of otic and epibranchial placodes in sub-dividing the posterior pre-placodal region [49, 1].

During their migration NC cells undergo developmental restrictions. However, it is generally accepted that populations of NC-derived stem cells (NCSCs) can be found within various niches throughout the adult body where they retain the capacity for self-renewal and multi-lineage differentiation [50, 51].

In the adult human body, populations of NCSCs can be found in various, easily accessible locations, such as teeth, inferior turbinate, and the palate [52-55]. Their developmental ability to differentiate into glial cells and neurons is conserved during adulthood [51, 56].

As shown by various studies, SCs from the NC can, furthermore, be found in both mouse and human hair follicles [57-61], of which the latter can be easily harvested using minimally invasive techniques. Differentiation of SCs derived from the hair follicle into smooth muscle cells, melanocytes, keratinocytes, osteocytes, and chondrocytes as well as glial cells, and, most importantly, neurons has been indicated in earlier studies [62-66]. In this thesis, we will investigate if hair follicle bulge-derived

SCs (HFBSCs) are able to migrate and differentiate into glial and neuronal cells *in vitro* (Chapters 2-4). Depending on these findings, NCSCs – and especially the relatively immune-privileged HFBSCs – might represent promising candidates for autologous SC therapies [67-69].

Due to the easy harvesting, efficient isolation and their *in vitro* differentiation potential, HFBSCs have advantages over SCs from other origins, such as neural progenitor cells or embryonic SCs. Nevertheless, the novelty of this type of stem cell in the field of regenerative therapy and particularly of inner ear cell-based therapy requires investigation of the differentiation and migration potential in the living animal, such as the mouse or the guinea pig.

The animal model and deafening

Guinea pigs have been used as experimental animals for centuries, which gave rise to the expression 'guinea pig' in English in the sense of a human experimental subject. Guinea pigs and humans share many biological similarities, such as a similar immune system, which led Robert Koch to discover in an 1882 study with guinea pigs that tuberculosis is caused by the bacterium *Mycobacterium tuberculosis* [70]. In addition, vitamin C was discovered in guinea pigs by means of nutritional deficiency, since guinea pigs like humans – and in contrast to most other animals – are incapable of endogenous synthesis of vitamin C, which leads to scurvy-like symptoms [71].

Moreover, the structure of the cochlea of guinea pigs is comparable to that of humans, demonstrating a more similar hearing range when compared to that of, e.g., mice, rats, gerbils, and cats. Therefore, guinea pigs have long been a preferred animal model in the field of hearing research. The anatomy of the guinea pig middle ear, allowing easy access to the round window and thus to the cochlea, further adds to its suitability. Another advantage of this animal model is the fact that the guinea pig permits xenogeneic transplants without induction of an immune rejection [72].

Altogether, these advantages are in favor of the guinea pig for cell-based regenerative therapy in the auditory system. Therefore, this could enable tracking of mouse-derived

HFBSCs after their implantation into the cochleas of deafened animals, in order to monitor their long-term survival, proliferation, and differentiation into functional SGNs. As explained earlier, SGNs are afferent neurons, that transmit electric signals encoding sound from the cochlear hair cells to the brain. They are classified as type-I (myelinated) SGNs - making up 90-95% of the total SGN population – and type-II (unmyelinated) SGNs (5-10%). Type-I SGNs innervate the inner hair cells within the organ of Corti, which are the primary sound receptors and, as such, are responsible for the sensation of hearing.

A potent drug for the induction of deafness is the selective Na^+/K^+-ATPase inhibitor ouabain (g-strophanthin), which has been reported to selectively destroy the type-I SGNs in certain species of rodent cochleas, while leaving type-II SGNs and cochlear hair cells unharmed. Contrary to deafening methods that are based upon systemic application of ototoxic drugs, this method uses local (i.e., deposition on RWM) instillation of the drug in order to bypass the blood-cochlea barrier. The advantage of this application approach is that ouabain does not interfere with the production of chemotactic growth factors of the hair and supporting cells. These growth factors may support survival of transplanted stem cells and may also direct peripheral projections of the newly formed neurons to the organ of Corti [73, 74].

The denervation effect of ouabain was initially observed in many studies using Mongolian gerbils [75-79] and was subsequently observed to occur as well in the cochlea of other rodent species, such as mice [80-84], rats [85-87], but also in cats [88], in a dose-dependent way.

However, comparably little is known about the effect of ouabain upon the guinea pig inner ear. Only two (contradictory) studies have described the morphological effect of local application of ouabain upon the SGNs in the guinea pig cochlea [89, 73]. It is hence necessary to evaluate if ouabain can be used for selective deafening of guinea pigs and subsequent regenerative stem cell therapy (Chapter 6).

Multimodal visualization

Following transplantation, it is necessary to track the transplanted cells in the living animal. Long-term follow-up studies of implanted cells give a closer insight into their survival, distribution in the inner ear and, ultimately, to their contribution to the regeneration of damaged structures.

Visualization of mammalian cells is used in a broad field of research: Investigation of engrafted cells, tracking of cancer cells in the mammalian organism, and the homing capacity of stem cells [90, 91]. Therefore, a range of different labeling techniques for mammalian cells has been developed, such as (i) genetic manipulation using a viral vector to introduce one or more reporter molecules (fluorescent or bioluminescent), and (ii) loading with superparamagnetic iron oxide (SPIO) and/or fluorescent nanoparticles, which enables multimodal imaging, but label the cells only temporarily.

More specifically, these labeling techniques enable imaging with different modalities, such as fluorescence imaging (FLI), bioluminescence imaging (BLI), and magnetic resonance imaging (MRI). Each one of these approaches has advantages and disadvantages and requires different imaging equipment. Multimodal imaging combining two or more of the above-mentioned modalities, offers the possibility of minimizing the potential drawbacks of using one single modality. This approach allows to make use of the modality-specific strengths and will help to optimize and complete the comprehension of graft behavior.

One approach to visualize cells is the use of naturally occurring fluorescent molecules, such as the green fluorescent protein (GFP), which can be used for both fluorescence microscopy and imaging. GFP was first described by Shimomura and colleagues in 1962 during the isolation of the bioluminescent protein aequorin from the luminous hydrozoan jellyfish *Aequorea victoria* as a byproduct [92, 93]. Since then, GFP and its numerous variants have become widely used tools for biological imaging in biochemistry and cell biology [93, 94]. Apart from jellyfish, other species were discovered expressing GFP-like proteins [95, 96]. Among these species are two copepod families in the class of Crustacea (phylum Arthropoda), which are known for expressing such GFP-like proteins, namely the *Pontellidae* and the *Aetideidae* [95, 97]. Advantages of copepod GFP (copGFP; λ_{ex}: 482nm, λ_{em}: 502nm) over other GFP variants are a high fluorescence quantum yield, which is more stable at a wide

range of temperatures (including 37°C, i.e. human body temperature) and features faster folding and post-translational maturation rates, resulting in rapid availability of the protein after transduction [98]. In addition, green fluorescence can be detected in copGFP-expressing cells during cell culture and in histological sections using conventional fluorescence microscopy. However, copGFP is not suitable for *in vivo* detection due to the low penetration depth of the excitation and emission light [92-94, 97].

This drawback of copGFP can be obviated by the use of expression of bioluminescent proteins, such as click beetle luciferase or firefly luciferase. Firefly luciferase and its visualization in single mammalian cells was first demonstrated by Hooper and colleagues [99]. As a result, visualization of cells using BLI became suitable for *in vitro* and *in vivo* studies. The firefly luciferase is an adenosine triphosphate (ATP)-dependent oxidoreductase, which specifically converts the substrate D-luciferin into oxyluciferin in the presence of molecular O_2, resulting in a bioluminescent signal emitting at a wavelength of 425–550 nm [100-102]. One of the most red-shifted naturally-occurring luciferases is derived from the head lanterns of the railroad worm, *Phrixothrix hirtus*, with $λ_{em}$ = 628 nm, which corresponds to (dark) orange [103]. The blue light-emitting luciferases Renilla and Gaussia are ATP-independent, but require coelenterazine as a substrate [104]. Furthermore, the blue-bioluminescent bacterial luciferase lux from *Photorhabdus luminescens* functions independent of substrate by auto-induction of luminescence [105-107]. Despite the fact that codon-optimized versions of lux were recently published, it remains difficult to express *P. luminescens* in mammalian cells [108, 109, 102].

Nonetheless, light in this range (blue to green) is particularly well-absorbed by tissue chromophores, such as (oxy-)hemoglobin, melanin and cytochromes in mammalian tissue, which leads to impracticality of these luciferases for *in vivo* imaging [110, 111]. However, the codon-optimized *Photinus pyralis* luciferase (Luc2) possesses major advantages in comparison to the wildtype luciferases, such as a high photon flux and an emission peak of 560 nm at 25°C [112]. At 37°C, a thermally induced shift towards 612 nm, which is above the light absorption spectrum of mammalian tissue, makes Luc2 a valuable tool for *in vivo* BLI [113]. Therefore, it is suitable for visualization of viable exogenous stem cells in the intact guinea pig cochlea using molecular optical imaging.

The lentiviral Luc2-copGFP reporter gene construct, which stably integrates into the genome of mammalian cells by means of viral transduction, leads to constitutive expression of Luc2 and copGFP at equimolar ratio, allowing FLI and BLI. Both imaging techniques, however, do not provide detailed anatomical information, nor do they enable visualization of transplanted cells. MRI, on the other hand, allows *in vivo* assessment of the exact location of transplanted cells, when loaded with SPIO nanoparticles and their migration within the host after engraftment. For dynamic evaluation of the migration of transplanted cells in deep tissue during *in vivo* experiments, SPIO nanoparticles have advantages due to their large signal contrast change [114]. Moreover, after sacrificing the animal, they can also be detected in histological sections using light and electron microscopy [115, 116].

Two examples of contrast-enhancing SPIO nanoparticles are ferumoxytol and NEO-STEM. Ferumoxytol is an U.S. Food and Drug Administration (FDA)-approved iron preparation for the treatment of anemia in chronic kidney disease [117]. With a straightforward cell-loading approach ferumoxytol effectively labels cells for *in vivo* MRI through formation of self-assembling nanocomplexes in the presence of heparin and protamine. NEO-STEM™ TMSR50 nanoparticles contain a magnetic core and a red-fluorescent dye, which allows visualization of nanoparticles using both MRI and FLI. The silica shell of NEO-STEM™ TMSR50 nanoparticles is biocompatible and resistant to degradation.

In conclusion, the fluorescent protein copGFP can be used to assess the transduction efficiency, for monitoring transduced cells *in vitro*, and in histological sections using conventional fluorescence microscopy. *In vivo*, viable cells can be detected by means of emitted light from the bioluminescent Luc2 after engraftment. This allows non-invasive long-term monitoring of cell viability and survival, while MRI of SPIO nanoparticle-loaded cells can be used to obtain additional anatomical information.

Aims and outline of this thesis

The general aim of this thesis is to investigate the feasibility of multimodal imaging techniques for the visualization of exogenous stem cells, i.e., HFBSCs, in the living animal. Due to the novelty of HFBSCs in this field of research, a series of proof-of-principle experiments have been undertaken *in vitro*, *ex vivo*/*in situ*, and *in vivo*:

Objective 1: *The isolation, expansion and neural differentiation of stem cells from human plucked hair* (Chapter 2).
This chapter examines whether HFBSCs still possess the immunophenotype of NCSCs and neural differentiation potential after isolation and expansion. In addition, it is investigated whether these cells support cryopreservation and tolerate needle shear-stress.

Objective 2: *Rule out the possible cytotoxic effects of lentiviral transduction and subsequent loading with nanoparticles on cell viability and proliferation of HFBSCs* in vitro (Chapter 3).
Prior to application of HFBSCs *in vivo*, the possible risk of negative effects of lentiviral transduction and loading with SPIO nanoparticles needs to be ruled out to obtain and maintain a viable cell population for cell-based regenerative therapy.

Objective 3: *Investigate the neuronal differentiation potential of HFBSCs in co-culture with modiolus explants from adult mice* (Chapter 4).
This chapter focuses on three key factors to ensure successful application of HFBSCs in cell-based therapy *in vivo*: (i) to ascertain the migratory character of the cells, (ii) to monitor their incorporation into damaged cochlear tissue lacking supportive growth factors from hair cells, and (iii) to assess their capability to undergo differentiation within a neural phenotype after integration into the modiolus explant.

Objective 4: *The feasibility of BLI for the visualization of transduced cells after engraftment in the intact guinea pig cochlea* (Chapter 5).
After excluding negative effects of the labeling methods, it is essential to assure that it is possible to image the labeled cells by means of BLI after transplantation in the inner ear of the guinea pig. This is particularly challenging since the cochlea of the guinea pig (our experimental animal model) is embedded within a bony otic capsule consisting of compact bone with a high mineral density, the bulla may block signal

detection during molecular FLI and BLI.

Objective 5: *Determine if the ototoxic drug ouabain results in selective degeneration of type-I SGNs in guinea pigs* (Chapter 6).
Due to two conflicting papers, we decide to re-investigate the ototoxic effect of ouabain application via the round window membrane of the cochlea and to study the validity of this protocol in the guinea pig.

Objective 6: *Multimodality imaging of HFBSCs in a mouse model of traumatic brain injury* (Chapter 7).
In this chapter we aim to establish that HFBSCs keep their neural differentiation potency after transplantation *in vivo*, and to investigate i) whether HFBSCs integrate into the brain, ii) whether they differentiate, and if so into which type of cell, and iii) whether they do not form extracellular matrix *in vivo*.

In Chapter 8, the results of our studies are discussed and future experiments will be considered, based upon the results presented in this thesis, to visualize HFBSCs in the cochlea of the guinea pig.

1

2

3

4

5

6

7

8

A

References

1. Steventon, B., Mayor, R., and Streit, A., Neural crest and placode interaction during the development of the cranial sensory system. Dev. Biol., 2014. **389**: pp. 28-38.
2. Huisman, M.A. and Rivolta, M.N., Neural crest stem cells and their potential application in a therapy for deafness. Front. Biosci. (Schol. Ed.), 2012. **4**: pp. 121-132.
3. Chen, J. and Streit, A., Induction of the inner ear: Stepwise specification of otic fate from multipotent progenitors. Hear. Res., 2013. **297**: pp. 3-12.
4. Pickles, J.O., *An introduction to the physiology of hearing*. Vol. Fourth Edition. 2013: Brill. 460 pages.
5. Kim, J. and Koo, M., Mass and stiffness impact on the middle ear and the cochlear partition. J. Audiol. Otol., 2015. **19**: pp. 1-6.
6. SMART, Servier Medical Art is licensed under CC BY 3.0. Les Laboratoires Servier: http://smart.servier.com.
7. Oghalai, J.S., The cochlear amplifier: Augmentation of the traveling wave within the inner ear. Curr. Opin. Otolaryngol. Head Neck Surg., 2004. **12**: pp. 431-438.
8. Pan, L. and Zhang, M., Structures of Usher syndrome 1 proteins and their complexes. Physiology, 2012. **27**: pp. 25-42.
9. Mulsow, J. and Reichmuth, C., The binaural click-evoked auditory brainstem response of the California sea lion (*Zalophus californianus*). J. Acoust. Soc. Am., 2013. **133**: pp. 579-586.
10. Burkard, R.F., Eggermont, J.J., and Don, M., *Auditory evoked potentials: Basic principles and clinical application*. 2007: Lippincott Williams & Wilkins. 731 pages.
11. Kraus, N. and Nicol, T., *Auditory evoked potentials*, in *Encyclopedia of neuroscience*, M.D. Binder, N. Hirokawa, and U. Windhorst, Editors. 2009, Springer Berlin Heidelberg. pp. 214-218.
12. Jewett, D.L. and Williston, J.S., Auditory-evoked far fields averaged from the scalp of humans. Brain, 1971. **94**: pp. 681-696.
13. Lev, A. and Sohmer, H., Sources of averaged neural responses recorded in animal and human subjects during cochlear audiometry (Electro-Cochleogram). Arch. klin. exp. Ohr.-, Nas.- u. Kehlk.-Heilk., 1972. **201**: pp. 79-90.
14. Huang, C.M., A comparative study of the brain stem auditory response in mammals. Brain Res., 1980. **184**: pp. 215-219.
15. Buchwald, J.S. and Huang, C., Far-field acoustic response: Origins in the cat. Science, 1975. **189**: pp. 382-384.
16. Achor, L.J. and Starr, A., Auditory brain stem responses in the cat. I. Intracranial and extracranial recordings. Electroencephalogr. Clin. Neurophysiol., 1980. **48**: pp. 154-173.
17. Wada, S.I. and Starr, A., Generation of auditory brain stem responses (ABRs). I. Effects of injection of a local anesthetic (procaine HCl) into the trapezoid body of guinea pigs and cat. Electroencephalogr. Clin. Neurophysiol., 1983. **56**: pp. 326-339.
18. Wada, S.I. and Starr, A., Generation of auditory brain stem responses (ABRs). III. Effects of lesions of the superior olive, lateral lemniscus and inferior colliculus on the ABR in guinea pig. Electroencephalogr. Clin. Neurophysiol., 1983. **56**: pp. 352-366.
19. Wada, S. and Starr, A., Anatomical bases of binaural interaction in auditory brain-stem responses from guinea pig. Electroencephalogr. Clin. Neurophysiol., 1989. **72**: pp. 535-544.
20. Dehmel, S., Eisinger, D., and Shore, S.E., Gap prepulse inhibition and auditory brainstem-evoked potentials as objective measures for tinnitus in guinea pigs. Front. Syst. Neurosci., 2012. **6**: pp. 1-15.
21. Ingham, N.J., Thornton, S.K., Comis, S.D., and Withington, D.J., The auditory brainstem response of aged guinea pigs. Acta Otolaryngol., 1998. **118**: pp. 673-680.
22. Yost, W.A., *Fundamentals of hearing: An introduction*. 2007: Academic Press.
23. Knipper, M., Van Dijk, P., Nunes, I., Ruttiger, L., and Zimmermann, U., Advances in the neurobiology of hearing disorders: recent developments regarding the basis of tinnitus and hyperacusis. Prog. Neurobiol., 2013. **111**: pp. 17-33.
24. Lang, H., *Loss, degeneration, and preservation of the spiral ganglion neurons and their processes*, in *The primary auditory neurons of the mammalian cochlea*, A. Dabdoub, *et al.*, Editors. 2016, Springer New York: New York, U.S.A. pp. 229-262.
25. Liberman, M.C., Epstein, M.J., Cleveland, S.S., Wang, H., and Maison, S.F., Toward a differential diagnosis of hidden hearing loss in humans. PLoS ONE, 2016. **11**: pp. e0162726.
26. Wu, P.Z., Liberman, L.D., Bennett, K., de Gruttola, V., O'Malley, J.T., and Liberman, M.C., Primary neural degeneration in the human cochlea: Evidence for hidden hearing loss in the aging ear. Neuroscience, 2018.
27. Briaire, J.J. and Frijns, J.H.M., The consequences of neural degeneration regarding optimal cochlear implant position in scala tympani: A model approach. Hear. Res., 2006. **214**: pp. 17-27.
28. Pickles, J.O., *An introduction to the physiology of hearing*. Vol. Third Edition. 2008.
29. Sherman, C. Closing the gap between cochlear implants and natural hearing. 2014 [cited 2018/03/06]; Available from: http://dana.org/News/Closing_the_Gap_Between_Cochlear_Implants_and_Natural_Hearing/.
30. Briaire, J.J., Cochlear implants: From model to patients, in Department Othorhinolaryngology. 2008, Leiden University Medical Center (LUMC), Leiden University: Leiden. pp. 281.
31. Stephen, J.O.L., Rachael, R.R., and Hugh, J.M., Principles of design and biological approaches for improving the selectivity of cochlear implant electrodes. J. Neural Eng., 2009. **6**: pp. 055002.
32. Pinyon, J.L., Tadros, S.F., Froud, K.E., AC, Y.W., Tompson, I.T., Crawford, E.N., Ko, M., Morris, R., Klugmann, M., and Housley, G.D., Close-field electroporation gene delivery using the cochlear implant electrode array enhances the bionic ear. Sci. Transl. Med., 2014. **6**: pp. 233ra54.
33. Nayagam, B.A., Human stem cells ameliorate auditory evoked responses in a model of neuropathy. Stem Cell Res. Ther., 2012. **3**: pp. 44.
34. Lemmens, R. and Steinberg, G.K., Stem cell therapy for acute cerebral injury: What do we know and what will the future bring? Curr. Opin. Neurol., 2013. **26**: pp. 617-625.
35. Hasan, A., Deeb, G., Rahal, R., Atwi, K., Mondello, S., Marei, H.E., Gali, A., and Sleiman, E., Mesenchymal stem cells in

the treatment of traumatic brain injury. Front. Neurol., 2017. **8**: pp. 1-15.

36. Verwoerd, C.D., van Oostrom, C.G., and Verwoerd-Verhoef, H.L., Otic placode and cephalic neural crest. Acta Otolaryngol., 1981. **91**: pp. 431-435.
37. Streit, A., Extensive cell movements accompany formation of the otic placode. Dev. Biol., 2002. **249**: pp. 237-254.
38. Bhattacharyya, S. and Bronner-Fraser, M., Hierarchy of regulatory events in sensory placode development. Curr. Opin. Genet. Dev., 2004. **14**: pp. 520-526.
39. Kuriyama, S. and Mayor, R., Molecular analysis of neural crest migration. Philos. Trans. R. Soc. Lond., B, Biol. Sci., 2008. **363**: pp. 1349-1362.
40. Ladher, R.K., O'Neill, P., and Begbie, J., From shared lineage to distinct functions: The development of the inner ear and epibranchial placodes. Development, 2010. **137**: pp. 1777-1785.
41. Groves, A.K. and LaBonne, C., Setting appropriate boundaries: Fate, patterning and competence at the neural plate border. Dev. Biol., 2014. **389**: pp. 2-12.
42. Streit, A. and Stern, C.D., Establishment and maintenance of the border of the neural plate in the chick: Involvement of FGF and BMP activity. Mech. Dev., 1999. **82**: pp. 51-66.
43. Litsiou, A., Hanson, S., and Streit, A., A balance of FGF, BMP and WNT signalling positions the future placode territory in the head. Development, 2005. **132**: pp. 4051-62.
44. McCabe, K.L. and Bronner-Fraser, M., Molecular and tissue interactions governing induction of cranial ectodermal placodes. Dev. Biol., 2009. **332**: pp. 189-195.
45. Kozlowski, D.J., Murakami, T., Ho, R.K., and Weinberg, E.S., Regional cell movement and tissue patterning in the zebrafish embryo revealed by fate mapping with caged fluorescein. Biochem. Cell Biol., 1997. **75**: pp. 551-562.
46. His, W., *Untersuchungen über die erste Anlage des Wirbelthierleibes: Die erste Entwickelung des Hühnchens im Ei*. Leipzig : F.C.W. Vogel, 1868: pp. 1-292.
47. Yoshida, S., Shimmura, S., Nagoshi, N., Fukuda, K., Matsuzaki, Y., Okano, H., and Tsubota, K., Isolation of multipotent neural crest-derived stem cells from the adult mouse cornea. Stem Cells, 2006. **24**: pp. 2714-2722.
48. Le Douarin, N.M., Calloni, G.W., and Dupin, E., The stem cells of the neural crest. Cell Cycle, 2008. **7**: pp. 1013-1019.
49. Theveneau, E., Steventon, B., Scarpa, E., Garcia, S., Trepat, X., Streit, A., and Mayor, R., Chase-and-run between adjacent cell populations promotes directional collective migration. Nat. Cell Biol., 2013. **15**: pp. 763-772.
50. Kruger, G.M., Mosher, J.T., Bixby, S., Joseph, N., Iwashita, T., and Morrison, S.J., Neural crest stem cells persist in the adult gut but undergo changes in self-renewal, neuronal subtype potential, and factor responsiveness. Neuron, 2002. **35**: pp. 657-669.
51. Kaltschmidt, B., Kaltschmidt, C., and Widera, D., Adult craniofacial stem cells: Sources and relation to the neural crest. Stem Cell Rev., 2012. **8**: pp. 658-671.
52. Fernandes, K.J., McKenzie, I.A., Mill, P., Smith, K.M., Akhavan, M., Barnabe-Heider, F., Biernaskie, J., Junek, A., Kobayashi, N.R., Toma, J.G., Kaplan, D.R., Labosky, P.A., Rafuse, V., Hui, C.C., and Miller, F.D., A dermal niche for multipotent adult skin-derived precursor cells. Nat. Cell Biol., 2004. **6**: pp. 1082-1093.
53. Techawattanawisal, W., Nakahama, K., Komaki, M., Abe, M., Takagi, Y., and Morita, I., Isolation of multipotent stem cells from adult rat periodontal ligament by neurosphere-forming culture system. Biochem. Biophys. Res. Commun., 2007. **357**: pp. 917-923.
54. Widera, D., Zander, C., Heidbreder, M., Kasperek, Y., Noll, T., Seitz, O., Saldamli, B., Sudhoff, H., Sader, R., Kaltschmidt, C., and Kaltschmidt, B., Adult palatum as a novel source of neural crest-related stem cells. Stem Cells, 2009. **27**: pp. 1899-1910.
55. Hauser, S., Widera, D., Qunneis, F., Müller, J., Zander, C., Greiner, J., Strauss, C., Lüningschrör, P., Heimann, P., Schwarze, H., Ebmeyer, J., Sudhoff, H., Araúzo-Bravo, M.J., Greber, B., Zaehres, H., Schöler, H., Kaltschmidt, C., and Kaltschmidt, B., Isolation of novel multipotent neural crest-derived stem cells from adult human inferior turbinate. Stem Cells Dev., 2012. **21**: pp. 742-756.
56. Liu, J.A. and Cheung, M., Neural crest stem cells and their potential therapeutic applications. Dev. Biol., 2016. **419**: pp. 199-216.
57. Sieber-Blum, M. and Grim, M., The adult hair follicle: Cradle for pluripotent neural crest stem cells. Birth Defects Res. C. Embryo Today, 2004. **72**: pp. 162-172.
58. Yu, H., Fang, D., Kumar, S.M., Li, L., Nguyen, T.K., Acs, G., Herlyn, M., and Xu, X., Isolation of a novel population of multipotent adult stem cells from human hair follicles. Am. J. Pathol., 2006. **168**: pp. 1879-1888.
59. Krejci, E. and Grim, M., Isolation and characterization of neural crest stem cells from adult human hair follicles. Folia. Biol. (Praha), 2010. **56**: pp. 149-157.
60. Yu, H., Kumar, S.M., Kossenkov, A.V., Showe, L., and Xu, X., Stem cells with neural crest characteristics derived from the bulge region of cultured human hair follicles. J Invest Dermatol 2010. **130**: pp. 1227-36.
61. Liu, F., Zhang, C., and Hoffman, R.M., Nestin-expressing stem cells from the hair follicle can differentiate into motor neurons and reduce muscle atrophy after transplantation to injured nerves. Tissue Eng. Part A, 2014. **20**: pp. 656-662.
62. Sieber-Blum, M., Grim, M., Hu, Y.F., and Szeder, V., Pluripotent neural crest stem cells in the adult hair follicle. Dev. Dyn., 2004. **231**: pp. 258-269.
63. Amoh, Y., Li, L., Katsuoka, K., Penman, S., and Hoffman, R.M., Multipotent nestin-positive, keratin-negative hair-follicle bulge stem cells can form neurons. Proc. Natl. Acad. Sci. USA, 2005. **102**: pp. 5530-5534.
64. El Seady, R., Huisman, M.A., Löwik, C.W., and Frijns, J.H.M., Uncomplicated differentiation of stem cells into bipolar neurons and myelinating glia. Biochem. Biophys. Res. Commun., 2008. **376**: pp. 358-362.
65. Amoh, Y., Kanoh, M., Niiyama, S., Hamada, Y., Kawahara, K., Sato, Y., Hoffman, R.M., and Katsuoka, K., Human hair follicle pluripotent stem (hfPS) cells promote regeneration of peripheral-nerve injury: An advantageous alternative to ES and iPS cells. J. Cell Biochem., 2009. **107**: pp. 1016-1020.
66. Clewes, O., Narytnyk, A., Gillinder, K.R., Loughney, A.D., Murdoch, A.P., and Sieber-Blum, M., Human epidermal neural crest stem cells (hEPI-NCSC)-characterization and directed differentiation into osteocytes and melanocytes. Stem Cell Rev., 2011. **7**: pp. 799-814.

67. Paus, R., Nickoloff, B.J., and Ito, T., A 'hairy' privilege. Trends Immunol., 2005. **26**: pp. 32-40.
68. Sieber-Blum, M. and Hu, Y., Epidermal neural crest stem cells (EPI-NCSC) and pluripotency. Stem Cell Rev., 2008. **4**: pp. 256-260.
69. Greiner, J.F., Hauser, S., Widera, D., Muller, J., Qunneis, F., Zander, C., Martin, I., Mallah, J., Schuetzmann, D., Prante, C., Schwarze, H., Prohaska, W., Beyer, A., Rott, K., Hutten, A., Golzhauser, A., Sudhoff, H., Kaltschmidt, C., and Kaltschmidt, B., Efficient animal-serum free 3D cultivation method for adult human neural crest-derived stem cell therapeutics. Eur. Cell Mater., 2011. **22**: pp. 403-419.
70. Koch, H.H.R., Die Aetiologie der Tuberculose. Berliner Klinische Wochenschrift, 1882. **15**: pp. 221-230.
71. Holst, A. and Frolich, T., Experimental studies relating to "Ship-beri-beri" and scurvy. J. Hyg. (Lond), 1907. **7**: pp. 634-671.
72. Regala, C., Duan, M., Zou, J., Salminen, M., and Olivius, P., Xenografted fetal dorsal root ganglion, embryonic stem cell and adult neural stem cell survival following implantation into the adult vestibulocochlear nerve. Exp. Neurol., 2005. **193**: pp. 326-333.
73. Cho, Y.B., Cho, H.H., Jang, S., Jeong, H.S., and Park, J.S., Transplantation of neural differentiated human mesenchymal stem cells into the cochlea of an auditory-neuropathy guinea pig model. J. Korean Med. Sci., 2011. **26**: pp. 492-498.
74. Chen, W., Jongkamonwiwat, N., Abbas, L., Eshtan, S.J., Johnson, S.L., Kuhn, S., Milo, M., Thurlow, J.K., Andrews, P.W., Marcotti, W., Moore, H.D., and Rivolta, M.N., Restoration of auditory evoked responses by human ES-cell-derived otic progenitors. Nature, 2012. **490**: pp. 278-282.
75. Schmiedt, R.A., Okamura, H.O., Lang, H., and Schulte, B.A., Ouabain application to the round window of the gerbil cochlea: A model of auditory neuropathy and apoptosis. J. Assoc. Res. Otolaryngol., 2002. **3**: pp. 223-233.
76. Lang, H., Schulte, B.A., and Schmiedt, R.A., Ouabain induces apoptotic cell death in type I spiral ganglion neurons, but not type II neurons. J. Assoc. Res. Otolaryngol., 2005. **6**: pp. 63-74.
77. Wang, L.E., Cao, K.L., Yin, S.K., Wang, Z., and Chen, Z.N., Cochlear function after selective spiral ganglion cells degeneration induced by ouabain. Chin. Med. J., 2006. **119**: pp. 974-979.
78. Qu, J., Gan, Y.N., Xie, K.L., Liu, W.B., Wang, Y.F., Hei, R.Y., Mi, W.J., and Qiu, J.H., Inhalation of hydrogen gas attenuates ouabain-induced auditory neuropathy in gerbils. Acta Pharmacol. Sin., 2012. **33**: pp. 445-451.
79. Bourien, J., Tang, Y., Batrel, C., Huet, A., Lenoir, M., Ladrech, S., Desmadryl, G., Nouvian, R., Puel, J.L., and Wang, J., Contribution of auditory nerve fibers to compound action potential of the auditory nerve. J. Neurophysiol., 2014. **112**: pp. 1025-1039.
80. Kilpatrick, L.A., Samuvel, D.J., Zhu, J., Smythe, N., and Lang, H., Ouabain-induced auditory nerve degeneration in congenic Ly5.1 mice. J. Otol., 2011. **6**: pp. 19-28.
81. Kilpatrick, L.A., Zhu, J., Lee, F.S., and Lang, H., Role of stromal cell-derived factor-1 expression in the injured mouse auditory nerve. Otolaryngol. Head Neck Surg., 2011. **145**: pp. 1007-1015.
82. Lang, H., Li, M., Kilpatrick, L.A., Zhu, J., Samuvel, D.J., Krug, E.L., and Goddard, J.C., Sox2 up-regulation and glial cell proliferation following degeneration of spiral ganglion neurons in the adult mouse inner ear. J. Assoc. Res. Otolaryngol., 2011. **12**: pp. 151-171.
83. Yuan, Y. and Chi, F., Dynamic changes in hair cell ribbon synapse induced by loss of spiral ganglion neurons in mice. Chin. Med. J. (Engl), 2014. **127**: pp. 1941-1946.
84. Yuan, Y., Shi, F., Yin, Y., Tong, M., Lang, H., Polley, D.B., Liberman, M.C., and Edge, A.S., Ouabain-induced cochlear nerve degeneration: Synaptic loss and plasticity in a mouse model of auditory neuropathy. J. Assoc. Res. Otolaryngol., 2014. **15**: pp. 31-43.
85. Fu, Y., Ding, D., Jiang, H., and Salvi, R., Ouabain-induced cochlear degeneration in rat. Neurotox. Res., 2012. **22**: pp. 158-169.
86. Qu, J., Huang, H., Wang, J., Mi, W.J., Qiao, L., and Qiu, J.H., Detrimental effects of ouabain on cochlear spiral ganglion cells in rats. Chin. J. Otorhinolaryngol. Head Neck Surg., 2012. **47**: pp. 926-930.
87. Wang, X., Wang, Y., Ding, Z.J., Yue, B., Zhang, P.Z., Chen, X.D., Chen, X., Chen, J., Chen, F.Q., Chen, Y., Wang, R.F., Mi, W.J., Lin, Y., Wang, J., and Qiu, J.H., The role of RIP3 mediated necroptosis in ouabain-induced spiral ganglion neurons injuries. Neurosci. Lett., 2014. **578**: pp. 111-116.
88. Kim, B.Y., Bae, W.Y., Kim, J.-R., and Lee, T.H., Damage of spiral ganglion cell induced by ouabain application in cat. Korean J. Otorhinolaryngol. Head Neck Surg., 2014. **57**: pp. 589-595.
89. Hamada, M. and Kimura, R.S., Morphological changes induced by administration of a Na+,K+-ATPase inhibitor in normal and hydropic inner ears of the guinea pig. Acta Otolaryngol., 1999. **119**: pp. 778-786.
90. Edinger, M., Sweeney, T.J., Tucker, A.A., Olomu, A.B., Negrin, R.S., and Contag, C.H., Noninvasive assessment of tumor cell proliferation in animal models. Neoplasia, 1999. **1**: pp. 303-310.
91. Kim, D.E., Schellingerhout, D., Ishii, K., Shah, K., and Weissleder, R., Imaging of stem cell recruitment to ischemic infarcts in a murine model. Stroke, 2004. **35**: pp. 952-957.
92. Shimomura, O., Johnson, F.H., and Saiga, Y., Extraction, purification and properties of aequorin, a bioluminescent protein from the luminous hydromedusan, Aequorea. J. Cell. Comp. Physiol., 1962. **59**: pp. 223-239.
93. Tsien, R.Y., The green fluorescent protein. Annu. Rev. Biochem., 1998. **67**: pp. 509-544.
94. Shaner, N.C., Steinbach, P.A., and Tsien, R.Y., A guide to choosing fluorescent proteins. Nat. Methods, 2005. **2**: pp. 905-909.
95. Shagin, D.A., Barsova, E.V., Yanushevich, Y.G., Fradkov, A.F., Lukyanov, K.A., Labas, Y.A., Semenova, T.N., Ugalde, J.A., Meyers, A., Nunez, J.M., Widder, E.A., Lukyanov, S.A., and Matz, M.V., GFP-like proteins as ubiquitous metazoan superfamily: evolution of functional features and structural complexity. Mol. Biol. Evol., 2004. **21**: pp. 841-850.
96. Masuda, H., Takenaka, Y., Yamaguchi, A., Nishikawa, S., and Mizuno, H., A novel yellowish-green fluorescent protein from the marine copepod, Chiridius poppei, and its use as a reporter protein in HeLa cells. Gene, 2006. **372**: pp. 18-25.
97. Hunt, M.E., Scherrer, M.P., Ferrari, F.D., and Matz, M.V., Very bright green fluorescent proteins from the pontellid copepod Pontella mimocerami. PLoS ONE, 2010. **5**: pp. e11517.
98. Evdokimov, A.G., Pokross, M.E., Egorov, N.S., Zaraisky, A.G., Yampolsky, I.V., Merzlyak, E.M., Shkoporov, A.N., Sander, I., Lukyanov, K.A., and Chudakov, D.M., Structural basis for the fast maturation of Arthropoda green fluorescent protein.

EMBO Rep., 2006. **7**: pp. 1006-1012.

99. Hooper, C.E., Ansorge, R.E., Browne, H.M., and Tomkins, P., CCD imaging of luciferase gene expression in single mammalian cells. J. Biolumin. Chemilumin., 1990. **5**: pp. 123-130.
100. Green, A.A. and McElroy, W.D., Crystalline firefly luciferase. Biochim. Biophys. Acta, 1956. **20**: pp. 170-176.
101. Contag, C.H. and Bachmann, M.H., Advances in *in vivo* bioluminescence imaging of gene expression. Annu. Rev. Biomed. Eng., 2002. **4**: pp. 235-260.
102. Mezzanotte, L., Que, I., Kaijzel, E., Branchini, B., Roda, A., and Löwik, C., Sensitive dual color *in vivo* bioluminescence imaging using a new red codon optimized firefly luciferase and a green click beetle luciferase. PLoS ONE, 2011. **6**: pp. e19277.
103. Viviani, V.R., Bechara, E.J., and Ohmiya, Y., Cloning, sequence analysis, and expression of active Phrixothrix railroad-worms luciferases: Relationship between bioluminescence spectra and primary structures. Biochemistry, 1999. 38: pp. 8271-8279.
104. Tannous, B.A., Kim, D.E., Fernandez, J.L., Weissleder, R., and Breakefield, X.O., Codon-optimized *Gaussia* luciferase cDNA for mammalian gene expression in culture and *in vivo*. Mol. Ther., 2005. **11**: pp. 435-443.
105. Frackman, S., Anhalt, M., and Nealson, K.H., Cloning, organization, and expression of the bioluminescence genes of *Xenorhabdus luminescens*. J. Bacteriol., 1990. **172**: pp. 5767-5773.
106. Contag, C.H., Contag, P.R., Mullins, J.I., Spilman, S.D., Stevenson, D.K., and Benaron, D.A., Photonic detection of bacterial pathogens in living hosts. Mol. Microbiol., 1995. **18**: pp. 593-603.
107. Wilson, T. and Hastings, J.W., Bioluminescence. Annu. Rev. Cell Dev. Biol., 1998. **14**: pp. 197-230.
108. Patterson, S.S., Dionisi, H.M., Gupta, R.K., and Sayler, G.S., Codon optimization of bacterial luciferase (*lux*) for expression in mammalian cells. J. Ind. Microbiol. Biotechnol., 2005. **32**: pp. 115-123.
109. Close, D.M., Patterson, S.S., Ripp, S., Baek, S.J., Sanseverino, J., and Sayler, G.S., Autonomous bioluminescent expression of the bacterial luciferase gene cassette (*lux*) in a mammalian cell line. PLoS ONE, 2010. **5**: pp. e12441.
110. Wilson, B.C., Jeeves, W.P., and Lowe, D.M., *In vivo* and *post mortem* measurements of the attenuation spectra of light in mammalian tissues. Photochem. Photobiol., 1985. **42**: pp. 153-162.
111. Mezzanotte, L., Fazzina, R., Michelini, E., Tonelli, R., Pession, A., Branchini, B., and Roda, A., *In vivo* bioluminescence imaging of murine xenograft cancer models with a red-shifted thermostable luciferase. Mol. Imaging Biol., 2010. **12**: pp. 406-414.
112. Mezzanotte, L., Aswendt, M., Tennstaedt, A., Hoeben, R., Hoehn, M., and Löwik, C., Evaluating reporter genes of different luciferases for optimized *in vivo* bioluminescence imaging of transplanted neural stem cells in the brain. Contrast Media Mol. Imaging, 2013. **8**: pp. 505-513.
113. Welsh, D.K. and Noguchi, T., Cellular bioluminescence imaging. Cold Spring Harb. Protoc., 2012. **2012**: pp. 852-866.
114. Sykova, E. and Jendelova, P., In vivo *tracking of stem cells in brain and spinal cord injury*, in *Progr. Brain Res.*, T.W. John and I.R.M. Andrew, Editors. 2007, Elsevier. pp. 367-383.
115. Jendelova, P., Herynek, V., DeCroos, J., Glogarova, K., Andersson, B., Hajek, M., and Sykova, E., Imaging the fate of implanted bone marrow stromal cells labeled with superparamagnetic nanoparticles. Magn. Reson. Med., 2003. **50**: pp. 767-776.
116. Bulte, J.W. and Kraitchman, D.L., Iron oxide MR contrast agents for molecular and cellular imaging. NMR Biomed., 2004. **17**: pp. 484-499.
117. Rosner, M.H. and Bolton, W.K., Ferumoxytol for the treatment of anemia in chronic kidney disease. Drugs Today (Barc), 2009. **45**: pp. 779-786.

1

2

3

4

5

6

7

8

A